Am J Physiol Endocrinol Metab 291: E323–E332, 2006.
First published March 28, 2006; doi:10.1152/ajpendo.00047.2006.

The vascular endothelial cell mediates insulin transport into skeletal muscle

Hong Wang, Zhenqi Liu, Guolian Li, and Eugene J. Barrett

Division of Endocrinology and Metabolism, Department of Internal Medicine, University of Virginia Health System, Charlottesville, Virginia

Submitted 31 January 2006; accepted in final form 21 March 2006

Wang, Hong, Zhenqi Liu, Guolian Li, and Eugene J. Barrett. The vascular endothelial cell mediates insulin transport into skeletal muscle. *Am J Physiol Endocrinol Metab* 291: E323–E332, 2006. First published March 28, 2006; doi:10.1152/ajpendo.00047.2006.—The pathways by which insulin exits the vasculature to muscle interstitium have not been characterized. In the present study, we infused FITC-labeled insulin to trace morphologically (using confocal immunohistochemical methods) insulin transport into rat skeletal muscle. We biopsied rectus muscle at 0, 10, 30, and 60 min after beginning a continuous (10 $mU \cdot min^{-1} \cdot kg^{-1}$), intravenous FITC-insulin infusion (with euglycemia maintained). The FITC-insulin distribution was compared with that of insulin receptors (IR), IGF-I receptors (IGF-IR), and caveolin-1 (a protein marker for caveolae) in skeletal muscle vasculature. We observed that muscle endothelium stained strongly for FITC-insulin within 10 min, and this persisted to 60 min. Endothelium stained more strongly for FITC-insulin than any other cellular elements in muscle. IR, IGF-IR, and caveolin-1 were also detected immunohistochemically in muscle endothelial cells. We further compared their intracellular distribution with that of FITC-insulin in cultured bovine aortic endothelial cells (bAECs). Considerable colocalization of IR or IGF-IR with FITC-insulin was noted. There was some but less overlap of IR or IGF-IR or FITC-insulin with caveolin-1. Immunoprecipitation of IR coprecipitated caveolin-1, and conversely the precipitation of caveolin-1 brought down IR. Furthermore, insulin increased the tyrosine phosphorylation of caveolin-1, and filipin (which inhibits caveolae formation) blocked insulin uptake. Finally, the ability of insulin, IGF-I, and IGF-I-blocking antibody to diminish insulin transport across bAECs grown on transwell plates suggested that IGF-IR, in addition to IR, can also mediate transendothelial insulin transit. We conclude that in vivo endothelial cells rapidly take up and concentrate insulin relative to plasma and muscle interstitium and that IGF-IR, like IR, may mediate insulin transit through endothelial cells in a process involving caveolae.

insulin action; insulin-like growth factor I receptor; insulin receptor; caveolae; immunocytochemistry

STUDIES OF THE KINETICS of insulin action on skeletal muscle (16, 17, 31, 32) suggest that its passage across the vascular wall to muscle interstitium may be rate limiting. Additionally, microdialysis and lymphatic sampling studies (4, 9, 10, 24, 25) suggest that insulin concentrations within the muscle interstitium remain at 50% or less of simultaneously measured plasma insulin even after prolonged insulin infusions. These observations suggest that insulin egress from the vasculature is a potentially important site for regulation of insulin action in muscle. Despite its potential importance, whether insulin exits the vasculature within muscle by a cellular or paracellular pathway has not been carefully defined morphologically. Clearly, endothelia from different tissues vary considerably in their permeability characteristics (22). The fenestrated endothelium of liver permits paracellular passage of proteins, and the kinetics of insulin's action on liver are much more rapid than in skeletal muscle (16). In contrast, skeletal muscle endothelium is considered "relatively tight;" i.e., occludens junctions potentially prevent paracellular transport of most macromolecules (22).

We have reported in a series of studies (19, 26, 27, 33) that insulin, at physiological concentrations, acts to increase the volume of microvasculature perfused within skeletal muscle by recruiting capillaries. We hypothesized that the additional endothelial surface made available by this recruitment would facilitate delivery of insulin and glucose to muscle interstitium. However, we recognize that insulin transfer to muscle interstitium occurs largely at the level of capillaries and that processes there might override any effect of insulin to increase endothelial surface area. The vascular endothelium expresses insulin receptors (IR) and even more abundant IGF-I receptors (IGF-IR). We (13) and others (5) have recently observed that the endothelial cell, like muscle and adipose, also possesses "hybrid" receptors composed of one insulin and one IGF-IR αβ-chain in the heterotetramer. Thus it appears reasonable to hypothesize that, besides IR (12), transendothelial insulin transport may also be mediated by IGF-IR and/or the hybrid receptors depending upon insulin concentrations.

A first step to examining insulin's handling by skeletal muscle endothelium appeared to be identifying the anatomic pathway by which insulin exits the vasculature into muscle interstitium. Careful electron microscopic autoradiographic studies by Bar et al. (1) suggested that insulin entered cardiac muscle interstitium via a transendothelial cell pathway that involved the insulin receptor. Comparable studies of skeletal muscle are not available. Given the known differences in the behavior of endothelium in different tissues (22), we set out to examine insulin's transendothelial transport in skeletal muscle using a fluorescent-labeled insulin and high-resolution confocal microscopy. We reasoned that the combination of confocal microscopy and fluorescent immunohistochemistry would allow us to address several questions in vivo. First, is FITC-insulin taken up by the endothelial cell within skeletal muscle? Second, does FITC-insulin associate with the IR or IGF-IR in the endothelial cell? Our initial findings led us to extend the study to examine FITC-insulin handling by cultured bovine aortic endothelial cells (bAECs) with a particular focus towards examining the relationship between insulin transport, caveolin-1, and the potential role of the IGF-IR in addition to the insulin receptor as a mediator of insulin uptake.

METHODS

Animal preparation. All procedures and protocols were approved by the University of Virginia's Animal Care and Use Committee.

Address for reprint requests and other correspondence: E. J. Barrett, Univ. of Virginia Health System, P. O. Box 801410, 450 Ray C. Hunt Drive, Charlottesville, VA 22908 (e-mail: ejb8x@virginia.edu).

The costs of publication of this article were defrayed in part by the payment of page charges. The article must therefore be hereby marked "*advertisement*" in accordance with 18 U.S.C. Section 1734 solely to indicate this fact.

Male Sprague-Dawley rats (250–300 g) were maintained in a 12:12-h light-dark cycle environment. The surgical process was as described previously (14). Briefly, following an overnight fast rats were anesthetized using pentobarbital sodium (50 mg/kg ip; Abbott Laboratories, North Chicago, IL). A midline neck incision was made, and the trachea and one external jugular vein and internal carotid artery were cannulated. The arterial catheter was connected through a three-way stopcock to a pressure probe, and heart rate and mean arterial pressure were monitored (Transonic Systems, Ithaca, NY). A continuous infusion of pentobarbital sodium was given at a variable rate to maintain a steady level of anesthesia during the experiment.

In vivo experimental protocols. After 30–45 min were allowed to obtain hemodynamic and anesthetic stability, a biopsy (~50 mg) was obtained from the rectus muscle and immediately placed in 10% neutralized buffered formalin (NBF). Thereafter, a euglycemic insulin clamp was carried out using FITC-insulin (Molecular Probes, Eugene, OR) at 10 $mU \cdot kg^{-1} \cdot min^{-1}$. Arterial blood glucose was monitored every 10 min throughout the insulin infusion, and 30% dextrose was infused at a variable rate to maintain the level of blood glucose within 10% of the basal. Three more biopsies were obtained from the rectus muscle (at 10, 30, and 60 min after the infusion was started, respectively), and the samples were immediately placed in 10% NBF for 48 h before being embedded in paraffin.

Cell culture. The bAECs (passage numbers 2–10; BioWhittaker, Walkersville, MD) were grown in slide chambers in EGMMV medium supplemented with human EGF, hydrocortisone, gentamicin, amphotericin, bovine brain extract, and 5% fetal bovine serum. The bAECs were incubated in serum-free basal medium for 16 h and then treated with 50 nM FITC-insulin in the basal medium for 30 min at 37°C with or without 5 μM unlabeled insulin (Humulin R; Eli Lilly, Indianapolis, IN), filipin (5 μg/ml; Sigma, St. Louis, MO), IGF-I (10 ng/ml; Sigma), IGF-IR neutralizing antibody (Ab-3, 1 μg/ml; Calbiochem, San Diego, CA), or nonspecific IgG (10 μg/ml; Santa Cruz Biotechnology, Santa Cruz, CA). Another group of bAECs was maintained in basal medium without FITC-insulin as a control. Cells were then fixed with cold methanol for 10 min at −20°C before immunocytochemical staining (see below) (18).

Transendothelial transport experiments. Cells were seeded onto the Transwell inserts (24 mm, 3-μm pore, Nucleopore polycarbonate membrane, tissue culture treated; Costar, Cambridge, MA) treated with human fibronectin. The transendothelial electrical resistances (TEERs) were monitored using an Epithelial Volt-ohmmeter (WPI EVOM) and EndOhm chamber (WPI EndOhm) after the confluent monolayer was formed. The TEERs peaked (10.7 ± 1.2 Ω/cm^2) at 96 h after the formation of confluent monolayers, and the plates with endothelial monolayers were then used for the insulin transport assays. After the cells had been washed twice at 37°C with phenol-free basal medium (EBM-NPR), the fluid in the top chamber was replaced with the basal medium containing FITC-insulin (100 nM) with or without 2 or 100 μM unlabeled insulin, 10 ng/ml IGF-I or 1 μg/ml IGF-IR neutralizing antibody, or 10 μg/ml nonspecific IgG. At preset intervals, 200 μl of fluid were removed from the bottom chamber, which was repleted with 200 μl of EBM-NPR to ensure hydrostatic balance. The concentrations of FITC-insulin were quantitated using a fluorometer (GENios; Tecan US, Durham, NC).

Immunoprecipitation and immunoblotting. Cultured bAECs were washed twice with ice-cold 1× PBS solution and then lysed and sonicated using a Fisher XL2020 sonicator (Fisher Scientific, Pittsburgh, PA) in ice-cold lysis buffer (50 mM Tris·HCl, pH 7.5, 150 mM NaCl, 1% NP-40, 0.25% sodium deoxycholate, 1 mM EGTA, 1 mM sodium orthovanadate, 1 mM NaF, 1 μg/ml aprotinin, 1 μg/ml leupeptin, 1 μg/ml pepstatin, and 1 mM PMSF). Cell lysates were centrifuged for 10 min at 4°C (20,000 *g*). Aliquots of supernatant containing 1,000 μg [for immunoprecipitation (IP) of IR β-subunit] or 2,000 μg (for IP of caveolin-1) of protein, respectively, in 1 ml of the lysis buffer were incubated with 25 μl of primary antibody against either IR β-subunit (1:400; Santa Cruz Biotechnology) or caveolin-1 (1:500; BD Transduction Laboratories) overnight at 4°C. Protein A/G plus IgG-agarose (Santa Cruz Biotechnology) was then added, and the mixture was kept at 4°C for 1 h with gentle rocking and then sedimented at 1,000 *g* for 30 s. After being washed six times with the lysis buffer, the beads were sedimented, resuspended in 50 μl of 2× sample buffer (375 mM Tris·HCl, pH 6.8, 12% SDS, 60% glycerol, 300 mM DTT, 0.06% bromophenol blue), and boiled for 5 min. The immunoprecipitants were electrophoresed on a 10% polyacrylamide gel. After being blocked with 5% low-fat milk in Tris-buffered saline plus Tween 20, membranes were incubated with antibody against IR β-subunit (1:1,000; Santa Cruz Biotechnology) or caveolin-1 (1:1,000; BD Transduction Laboratories,) for 1 h at 4°C. This was followed by incubation with species-specific secondary antibodies coupled to horseradish peroxidase (1:3,000; Santa Cruz Biotechnology), and the blots were developed using an enhanced chemiluminescence Western blotting kit (Amersham Life Sciences, Piscataway, NJ).

To confirm the identification of caveolin-1 in the anti-IRβ immunoprecipitate, the precipitate was run on a 10% gel and then silver-stained, the band running near 21 kDa was cut from the gel (along with 3 control pieces at different molecular masses), and the proteins were sequenced by mass spectrometry using a Finnigan LCQ ion trap mass spectrometer system with a Protana nanospray ion source interfaced to a self-packed 8 cm × 75 μm ID Phenomenex Jupiter 10-μm C_{18} reversed-phase capillary column. The data were analyzed by database searching using the Sequest search algorithm. Peptides that were not matched by this algorithm were interpreted manually and searched vs. the expressed sequence tag databases using the Sequest algorithm.

Histology. The paraffin-embedded tissues were sectioned at a thickness of 5 μm. The double-staining protocols were the same as we described previously (29, 30). Briefly, the paraffin-embedded sections or the methanol-fixed bAECs in the slide chamber were washed three times in PBS, permeabilized in PBS containing Triton X-100 (0.05% for the cultured cells and 0.3% for the paraffin-embedded sections) and 1% horse or goat serum for 30 min at room temperature, and incubated with two different primary antibodies against two different target proteins (double labeling) overnight at 4°C. The following primary antibodies were used: rabbit polyclonal antibody against caveolin-1 (1:200; Santa Cruz Biotechnology); mouse monoclonal anti-caveolin-1 (1:25; BD Transduction Laboratories); rabbit polyclonal anti-fluorescein (FITC) (1:100; Molecular Probes, Eugene, OR); mouse monoclonal anti-FITC (1:500; Molecular Probes); rabbit polyclonal anti-IR β-subunit (1:50; Upstate, Lake Placid, NY); mouse monoclonal anti-IR β-subunit (1:50; Chemicon International, Temecula, CA); rabbit polyclonal anti-IGF-IR β-subunit (1:50; Santa Cruz Biotechnology); and guinea pig polyclonal anti-human insulin (1:100; Chemicon). The cells were washed three times in PBS and then incubated with species-specific secondary antibodies conjugated with a fluorochrome at 1:200 dilutions for 45 min at room temperature. The following secondary antibodies were used: donkey anti-rabbit IgG conjugated to Cy2 or Cy3 (Jackson ImmunoResearch, West Grove, PA); donkey anti-mouse IgG conjugated to Cy2 or Cy3; and goat anti-mouse IgG_{2a} conjugated to Alexa 488 (Molecular Probes). The cells were washed three times in PBS and then coverslipped with the antifade mounting medium.

Imaging. The double immunocytochemical labeling was examined simultaneously using a two-color Olympus BX50 WI confocal microscope equipped with a krypton and argon laser, as described previously (29). The images were acquired at a resolution of 1,024 × 1,024 pixels and stored in 24-bit tagged image format file format. Fluorescence intensity of individual cells reflecting FITC-insulin uptake was quantified using Image J software (National Institutes of Health).

Statistical analysis. Data are presented as means ± SE. Statistical comparisons among different groups were made using two-way ANOVA. Statistical significance was defined as $P \leq 0.05$.

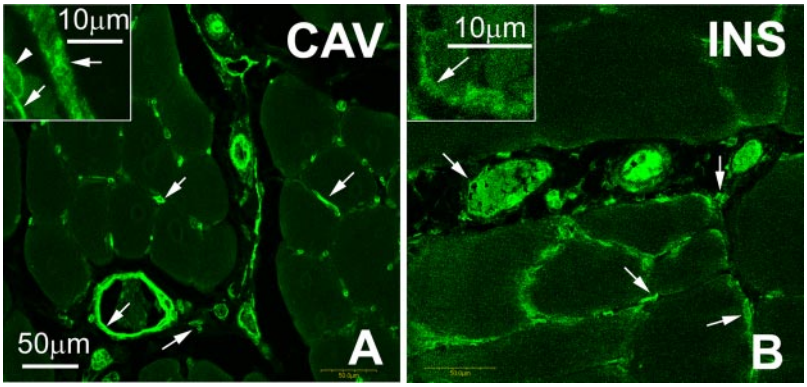

Fig. 1. Confocal images showing blood vessels labeled by caveolin-1 (CAV) immunoreactivity. *A*: low-magnification image showing CAV (revealed by Cy2)-labeled capillaries, arterioles, and venules. *Inset*: high-magnification image showing a venule labeled by CAV immunoreactivity. *B*: low-magnification image showing FITC-insulin (INS; revealed by Alexa 488)-labeled smaller arterioles and venules as well as capillaries. *Inset*: high-magnification image showing a venule labeled with anti-INS. Arrowheads point to nuclei of endothelial cells. Arrows point to the labeled vessels.

RESULTS

Caveolin-1, FITC-insulin, IR, and IGF-IR immunoreactivities are each enriched in the muscle vascular endothelium. Caveolae are abundant in continuous vascular endothelia (21). Caveolin-1, a 21-kDa membrane-associated protein, has been identified as a marker protein of caveolae in many cells (e.g., adipocytes, smooth muscle, and endothelial cells) but not appreciably in skeletal muscle. Figure 1*A* shows that anti-caveolin-1 immunoreactivity selectively labels the blood vessels in the rat skeletal muscle tissue. Caveolin-1 immunoreactivity stains the endothelial layer (Fig. 1*A*, *inset*) in even the smaller venules and capillaries as well as in deeper layers of the vessel wall in larger vessels. There was no clear immunoreactivity for caveolin-1 associated with myocytes or muscle interstitium. This was expected, because skeletal muscle is thought to express caveolin-3 but not caveolin-1. Similarly, the immunoreactivity to FITC-insulin was also seen in the endothelial layer (Fig. 1*B*, *inset*) of smaller arterioles and venules, as well as capillaries (Fig. 1*B*).

The distribution of FITC-insulin within skeletal muscle was examined in rectus biopsies obtained before and at 10, 30, and 60 min after the FITC-insulin clamp was begun (Fig. 2). Prior to its infusion, fluorescence attributable to FITC-insulin was absent. By comparison, intense staining with FITC-insulin was seen in the innermost layer of the blood vessel wall within 10 min, as revealed by anti-FITC antibody. Sections obtained at 30 and 60 min did not reveal any obvious increase in FITC-insulin signal intensity within the vessel wall as time progressed. The FITC-insulin appeared to concentrate within the innermost layer of the vessel wall in arterioles, venules, and capillaries (Fig. 2, *insets*; also see Figs. 3*E* and 4*A*), consistent with its being within the endothelial cells. At all times, FITC-insulin immunoreactivity was substantially stronger in the cytoplasm of vascular endothelium relative to either the intra-

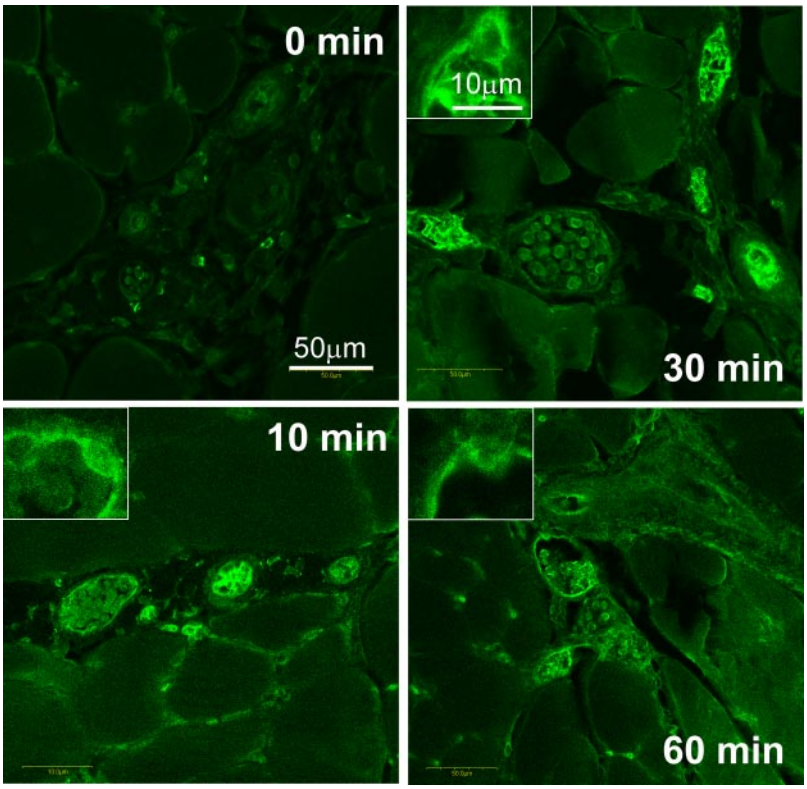

Fig. 2. Confocal images showing time course for tissue labeling with iv infused FITC-insulin [revealed by Alexa 488 (green)]. Prior to infusion of FITC-insulin, there was faint background staining, whereas by 10 min after a continuous iv infusion of FITC-insulin was begun the vascular lining was stained in capillaries, venules, and arterioles. *Insets* demonstrate that the staining is most intense within the endothelial cell layer of the vessel wall.

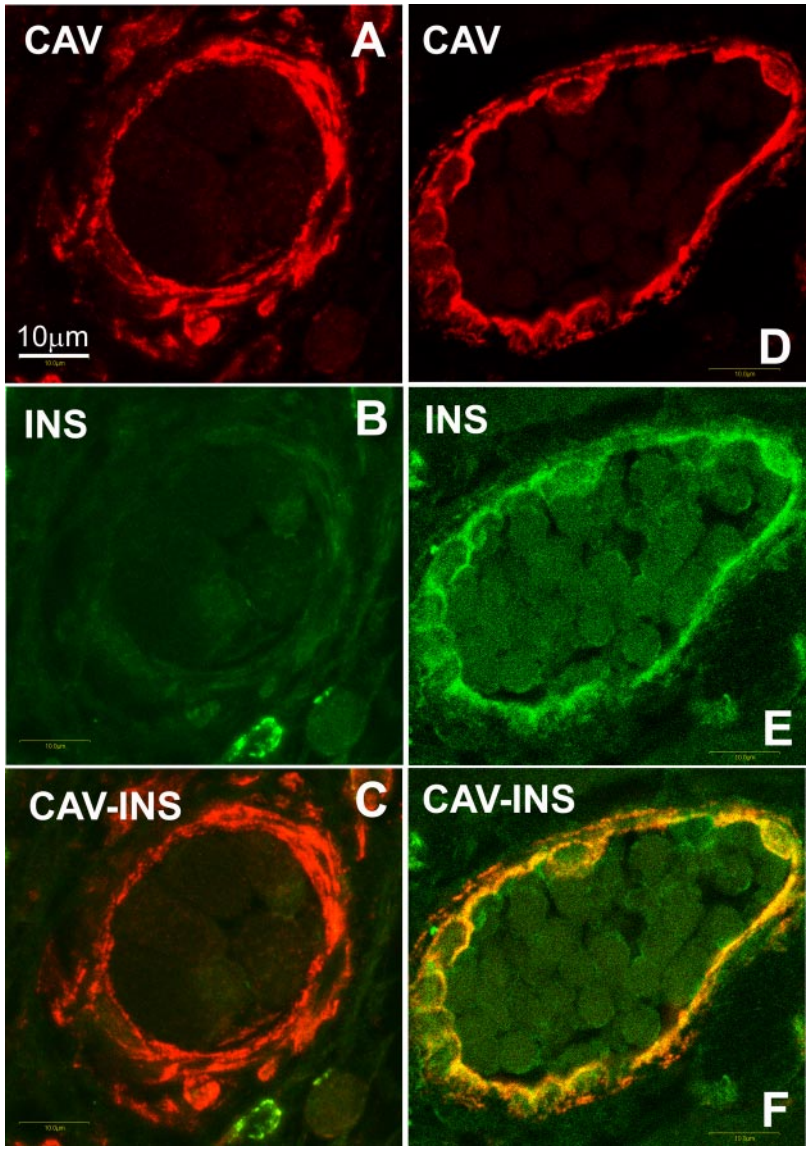

Fig. 3. Confocal images showing relationship between CAV and INS. *A–C* were obtained prior to infusion of INS, whereas *D–F* were obtained 10 min after a continuous iv infusion of INS was begun. *C* and *F* illustrate the colocalization.

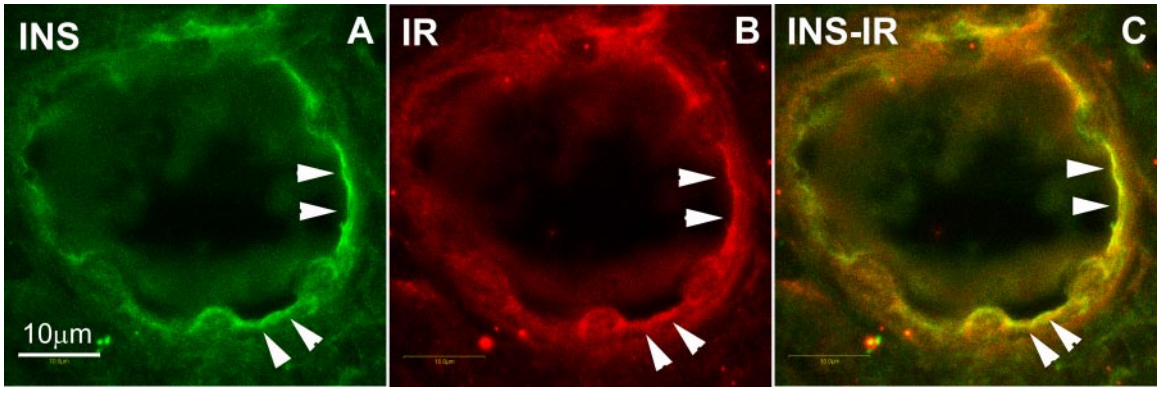

Fig. 4. Confocal images showing relationship between INS [revealed by Alexa 488 (green)] and the insulin receptor [IR, revealed by Cy3 (red)] in a small venule (from a biopsy obtained 30 min after the INS infusion was begun). Clearly, insulin was concentrated in and broadly distributed through the endothelial cells. There was a corresponding staining intensity between INS and the IR. Note that the staining was excluded from the nuclei of the endothelium and the deeper layers of the vascular wall. Arrowheads point to areas of colocalization.

vascular or interstitial space or the muscle cell. FITC-insulin also appeared to be excluded from cellular elements in the outer layers of larger arterioles and veins (Figs. 2 and 3*E*).

The relationship between caveolin-1 and infused FITC-insulin in vascular endothelium was further examined. Figure 3, *A–C*, shows the image of a blood vessel in muscle prior to infusion of FITC-insulin. In images obtained from biopsies taken 10 min after the infusion of FITC-insulin was started, the profile of endothelial and supporting layers of the blood vessel wall were again clearly outlined by caveolin-1 immunoreactivity (Fig. 3*D*). However, compared with baseline (Fig. 3*B*), intense staining with FITC-insulin was seen within the blood vessel wall within 10 min (Fig. 3*E*), as revealed by anti-FITC antibody. The merged image (Fig. 3*F*) highlights the colocalization between caveolin-1 and FITC-insulin. The observation that FITC-insulin is abundant in the endothelium of the vessel walls of small arterioles, venules, and capillaries but not significantly seen in the other layers of the vessel wall or in the surrounding tissue suggests that the endothelium imposes a barrier to insulin's entry into muscle. Interestingly, some signal from FITC-insulin was also apparent in association with the blood cells in the vascular lumen, suggesting that FITC-insulin was associated with blood cells during vascular transit. The intensity of the FITC-insulin labeling within the endothelium (relative to the muscle interstitium) suggests that it may be concentrated or bound at that site. In addition, within a number of sections there was a good correspondence between the localization and intensity of immunoreactivity associated with IR and FITC-insulin in the endothelial layer of the vascular wall (Fig. 4, *A–C*). FITC-insulin and IR were largely excluded from the nuclei of the vascular endothelium (Fig. 4).

Fig. 5, *A–C*, illustrates the relationship between IGF-IR and caveolin-1 within the endothelial layer of the vascular wall. Figure 5, *A* and *D*, shows that IGF-IR stained strongly within the endothelium of the vascular wall, although some staining can also be seen in the intravascular or interstitial space, the muscle cell, and the blood cells in the vascular lumen. Likewise, caveolin-1 (Fig. 5*B*) and FITC-insulin (Fig. 5*E*) were strongly labeled in the same endothelial layer. There was a clear overlap in the distribution throughout the innermost layer of the microvascular wall in skeletal muscle between the

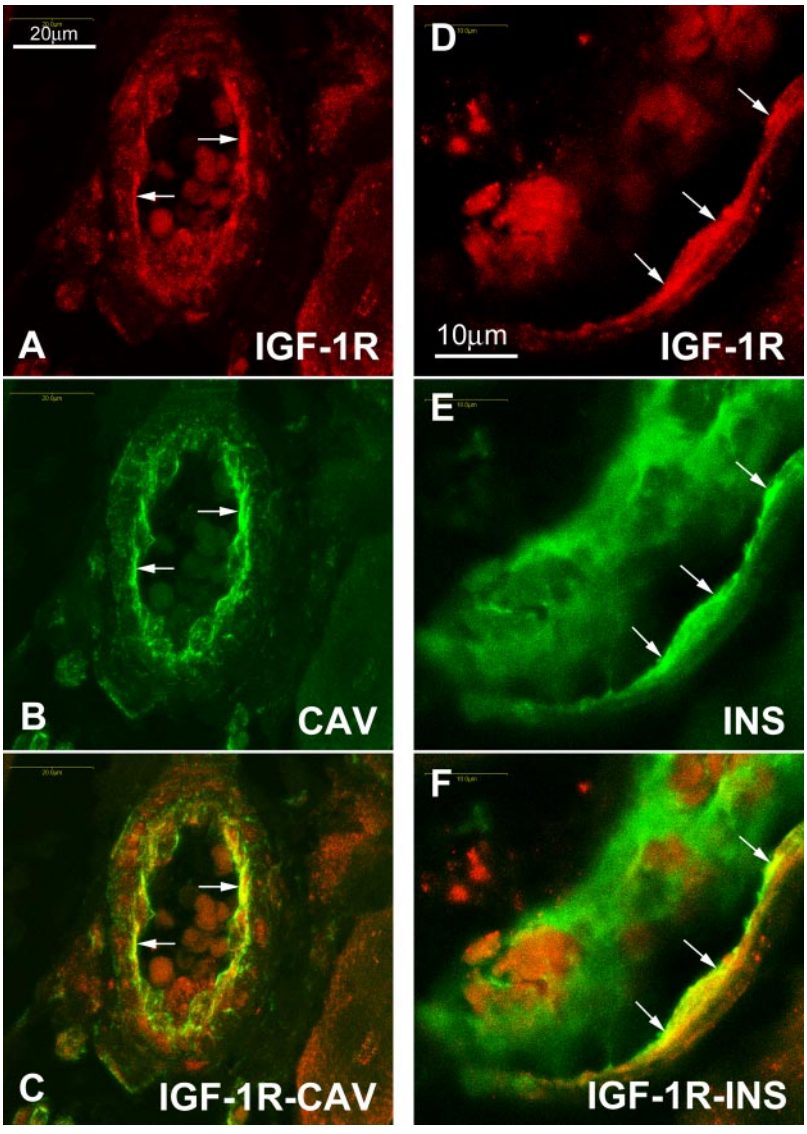

Fig. 5. Confocal images (from a biopsy 30 min after the INS infusion was begun) showing the relationship between IGF-I receptor [IGF-IR; revealed by Cy3 (red); *A*] and CAV [revealed by Cy2 (green); *B*] as well as the relationship between IGF-IR [revealed by Cy3 (red); *D*] and INS [revealed by Alexa 488 (green); *E*]. *C* (merged *A* and *B*) and *F* (merged *D* and *E*): there was an overlapping distribution of staining intensity in the endothelial layer. Arrows point to areas of colocalization.

IGF-IR and caveolin-1 as well as between the IGF-IR and FITC-insulin.

Colocalization of FITC-insulin, IR, IGF-IR, and caveolin-1 in cultured bAECs. The flattened, elongated nature of the endothelial cells within the vessel wall limits analysis of the anatomic relationships between cellular elements at the light microscope level. This limitation is less severe with cultured bAECs, where cells can be captured "en face". Figure 6, *B* and *E*, illustrates that, in cultured bAECs, fluorescence from FITC-insulin was relatively strong in the perinuclear region and at discrete foci throughout the cytosol as well as at the plasma membrane. The staining pattern of IR extensively overlapped with that of FITC-insulin (Fig. 6*A*). Overlapping, discrete, punctate labeling for both IR and FITC-insulin could be seen in many cells. The double staining revealed that the labeling of FITC-insulin appeared to colocalize with that of IR (Fig. 6*C*). The staining pattern of IGF-1R was similar to that of IR (Fig. 6*D*). Moreover, the colocalization between IGF-IR and FITC-insulin was more abundant than that of IR and FITC-insulin (Fig. 6, *C* and *F*).

Figure 7 shows the results of double staining of FITC-insulin and caveolin-1, IR and caveolin-1, as well as IGF-IR and caveolin-1 in cultured bAECs. Insulin, IR, and IGF-IR immunoreactivity considerably overlapped that of caveolin-1 both in the cytosol and at the cell membrane (Fig. 7, *C*, *F*, and *I*). Again, it appears that the colocalization between IGF-IR and caveolin-1 was more abundant than that of IR and caveolin-1. Serial optical sections through individual endothelial cells confirmed that insulin, caveolin-1, IR, and IGF-IR were present both in the cytosol and at the cell periphery (data not shown).

To further examine whether IR and caveolae are physically contiguous in endothelial cells, we performed two additional studies. Intact endothelial cells were lysed and then immunoprecipitated with either anti-IRβ or anti-caveolin-1 and then immunoblotted with anti-caveolin-1 or anti-IRβ. As shown in Fig. 8, each protein coimmunoprecipitated with the other. To further confirm that caveolin-1 was indeed associated with the IR, we performed mass spectrometric analysis of IR immunoprecipitates and identified the presence of four peptides that

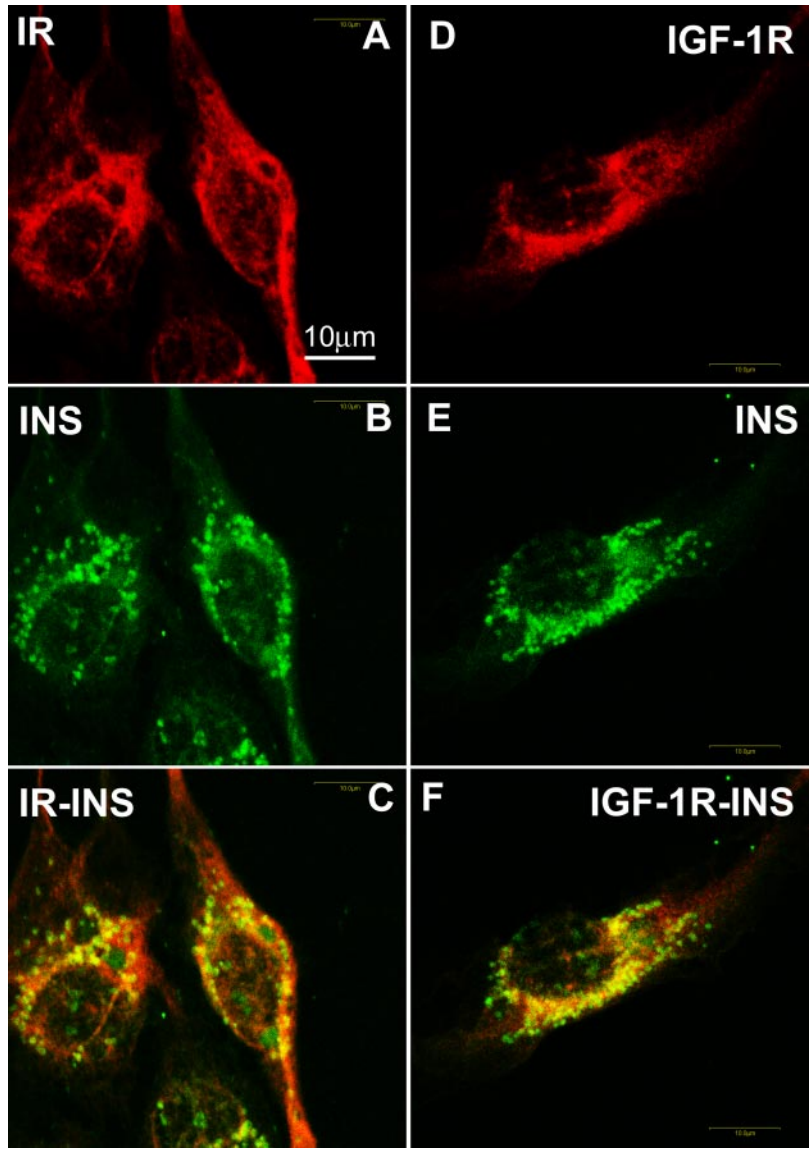

Fig. 6. Confocal images showing relationship between IR [revealed by Cy3 (red); *A*] and INS [revealed by Alexa 488 (green); *B*] as well as the relationship between IGF-IR [revealed by Cy3 (red); *D*] and INS [revealed by Alexa 488 (green); *E*]. *C* (merged *A* and *B*) and *F* (merged *D* and *E*): there was an overlapping distribution of staining intensity in punctuate areas in the cell cytosol.

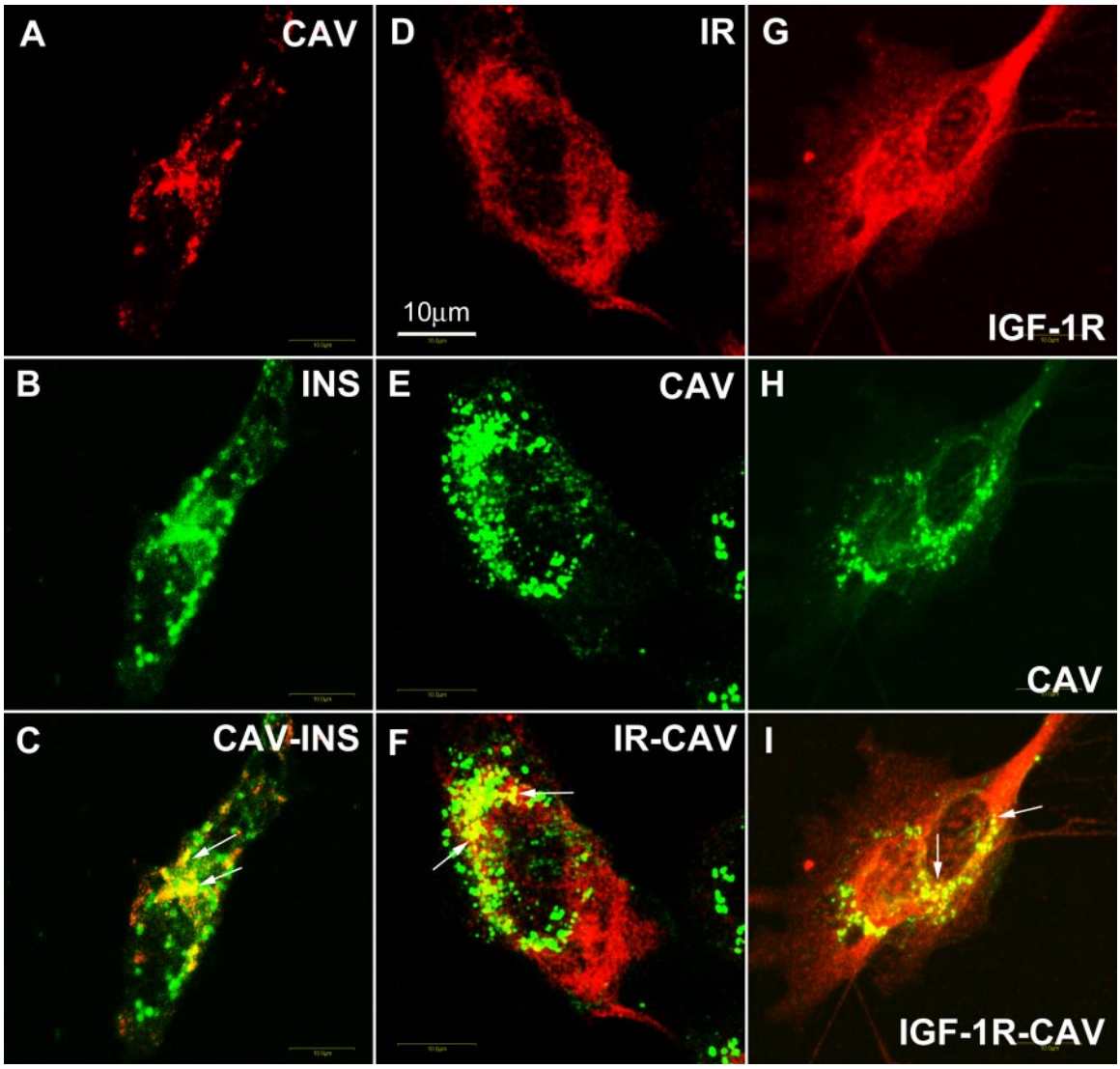

Fig. 7. Confocal images comparing cellular localization of CAV [revealed by Cy3 (red)] and internalized INS [revealed by Alexa 488 (green); *A–C*], IR [revealed by Cy3 (red)] and CAV [revealed by Cy2 (green); *D–F*], and IGF-IR [revealed by Cy3 (red)] and CAV [revealed by Cy2 (green); *G–I*] in cultured bovine aortic endothelial cells (bAECs). Arrows point to the areas of colocalization.

cover 21% of the caveolin-1 sequence. We also examined whether insulin treatment of bAECs affects the phosphorylation of caveolin-1. We found that, as has been described in adipocytes, in the endothelial cells, insulin (10 nM) increased caveolin phosphorylation on Western blots (data not shown).

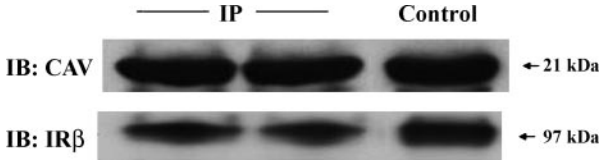

Fig. 8. CAV and IR coimmunoprecipitate with each other in cultured bAECs. *Top*: bAEC lysates were immunoprecipitated with anti-IRβ antibody, and Western blots were probed with anti-CAV. Purified CAV served as a positive control. *Bottom*: bAEC lysates were immunoprecipitated with anti-CAV, and Western blots were probed with anti-IRβ, with IRβ serving as a control. IP, immunoprecipitation.

Inhibition of bAEC FITC-insulin uptake and transport by unlabeled insulin, IGF-I, and IGF-IR neutralizing antibody. Figure 9*A* shows the inhibitory effects of either native insulin or filipin on FITC-insulin uptake by bAECs. Within 30 min of FITC-insulin exposure, the bAECs avidly accumulated FITC-insulin. Unlabeled insulin (μM) significantly inhibited the uptake of FITC-insulin ($P < 0.0001$). This finding is reminiscent of the inhibition of transendothelial insulin transport reported previously (12). Filipin (5 μg/ml), which disrupts lipid raft formations, also significantly reduced the uptake of FITC-insulin ($P < 0.0001$). Figure 9*B* shows the inhibitory effects of either IGF-I peptides or neutralizing antibody against IGF-IR on FITC-insulin uptake by bAECs. After 30 min of exposure to FITC-insulin, the bAECs were robustly stained both on the plasma membrane and in the cytosol. Unlabeled insulin (μM) and 10 ng/ml IGF-I each significantly inhibited the uptake of FITC-insulin by bAECs ($P < 0.0001$). Blocking antibody to the IGF-IR also significantly diminished the uptake

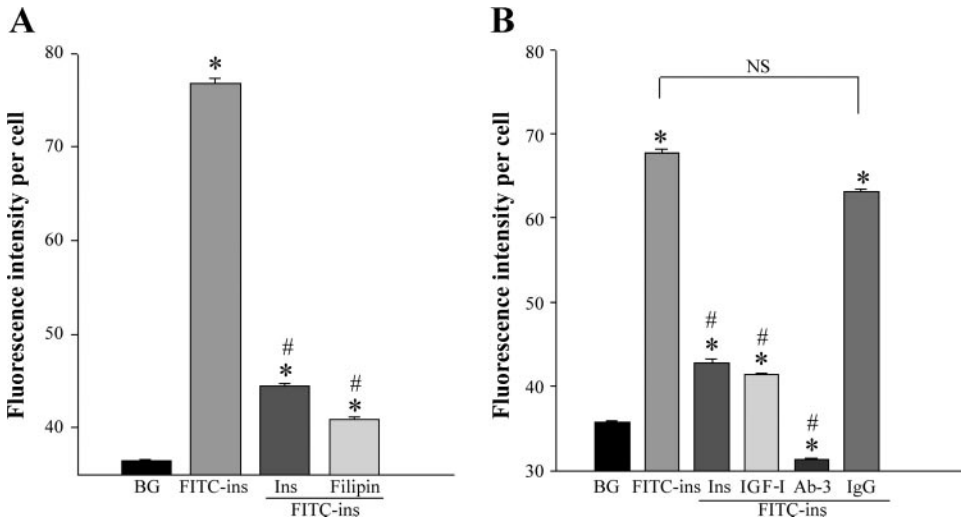

Fig. 9. *A*: effects of native insulin and filipin on FITC-insulin uptake by bAECs. Cells were incubated with either basal medium (BG) or FITC-insulin only or FITC-insulin plus 5 μM native insulin (Ins) or FITC-insulin and 5 μg/ml filipin for 30 min before the immunocytochemical staining using anti-FITC antibody (see METHODS). Fluorescence intensity reflecting FITC-insulin uptake by individual cells from different groups was measured on respective confocal images (30 cells were measured for each group). $*P < 0.05$ vs. BG; $\#P < 0.0001$ vs. FITC-insulin alone. *B*: effects of IGF-I peptides and the blocking antibody against IGF-IR on FITC-insulin uptake by bAECs. Cells were incubated with either BG or FITC-insulin only or FITC-insulin in the presence of either 5 μM native insulin or 10 ng/ml IGF-I or IGF-IR neutralizing antibody (Ab3) or nonspecific IgG for 30 min before the immunocytochemical staining using anti-FITC antibody (see METHODS). Fluorescence intensity reflecting FITC-insulin uptake by individual cells from different groups was measured on respective confocal images (33 cells were measured for each group). $*P < 0.0001$ vs. BG; $\#P < 0.0001$ vs. FITC-insulin alone; NS, $P > 0.05$.

($P < 0.0001$) whereas nonspecific IgG was without effect ($P > 0.05$).

Figure 10 illustrates the diminished transendothelial transport of FITC-insulin provoked by adding high concentrations of unlabeled insulin to bAECs grown on Transwell plates (*A*). Both IGF-I and blocking antibody to the IGF-IR likewise diminished transendothelial insulin transport (*B*); however, a nonspecific IgG (10 μg/ml) had no effect on the transport (data not shown). As a control, 50 nM FITC-inulin was added to the Transwell upper chamber, and we observed that, at 120 min, inulin transfer across the endothelial cells averaged <30% of that observed for FITC-insulin.

DISCUSSION

The results presented here provide the first clear evidence that in vivo insulin rapidly (within 10 min) enters the vascular endothelial cell within mammalian skeletal muscle. We are not aware of previous studies examining the time course for insulin entry into the endothelial cell or the anatomic pathway by which insulin exits the vasculature within skeletal muscle. Bar et al. (1) observed that within 2 min after adding ^{125}I-labeled insulin to the perfusate of an isolated rat heart, the endothelial cells and subsequently cardiac muscle interstitium were labeled. Interestingly, in that study, in addition to observing a rapid uptake of ^{125}I-insulin by the endothelial cell, the investigators also reported that the intensity of labeling of the endothelial cell was >10-fold above that of muscle interstitium. The investigators confirmed that ^{125}I in heart tissue was 80–90% still in the form of ^{125}I-insulin. Similarly, there is good evidence that FITC-insulin is not degraded in tissue or in cultured cells, and therefore, the FITC immunoreactivity observed within both vessel walls in vivo and cultured cells in vitro in essence represents the FITC-insulin distribution. The findings strongly indicate that skeletal muscle endothelium takes up insulin rapidly and avidly and that insulin is concentrated in endothelium relative to either the vascular or interstitial space or the myocytes. Studies by Miles et al. (16) suggested that the $t_{1/2}$ for insulin entry into muscle interstitium is on the order of 20 min in the rat. If insulin is indeed traversing the endothelium via a transcellular route, and if transit of insulin into the interstitium is a limiting step for insulin action, the rapid appearance of insulin in the endothelial

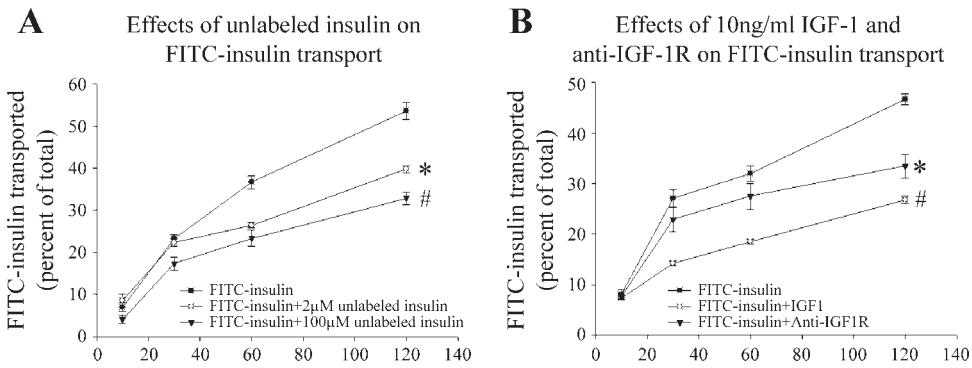

Fig. 10. *A*: time course for the movement of FITC-insulin across endothelial cells cultured on Transwell plates. Cells were exposed to 100 nM FITC-insulin alone or in the presence of either 2 or 100 μM unlabeled insulin. *B*: time course for the transport of labeled insulin across the endothelium in the absence and presence of either 10 ng/ml IGF-I or neutralizing antibody to the IGF-IR. $*P < 0.05$; $\#P < 0.02$ vs. FITC-insulin alone.

cell may point to either the movement of insulin across the cell or its release at the ablumenal side as potentially slow steps.

In the present study we elected to use a fluorescent-tagged insulin and confocal microscopy, recognizing that our spatial resolution would be less than with electron microscopy (EM) but that it offered the advantage of directly comparing the tissue/cellular localization of insulin with its receptor and with caveolin-1 by use of immunohistochemical methods. The most detailed electron microscopic study of transendothelial insulin transport was reported by Bendayan and Razio (2) in studies of the perfused rete mirable of the eel swim bladder. Using an immunogold method, they reported that insulin traversed the endothelium via a tubular-vesicular transcytotic pathway. However, in that study the authors commented that the efficiency of labeling required that insulin be used at a very high concentration (~1 mM). As a result, it is difficult to discern whether the transport pathway observed represents that which would be pertinent at more physiological insulin concentrations. It also remains possible that the behavior of endothelium in the eel swim bladder differs from that of mammalian skeletal muscle. The insulin infusion rate used (10 $mU \cdot min^{-1} \cdot kg^{-1}$) in the present study is sufficient to raise the plasma insulin to ~2 nM. This is comparable to a high physiological range and is typical of the insulin concentrations encountered in states of insulin resistance, such as in the Zucker rat (28). It is greater than five orders of magnitude lower than was used for the previous EM study.

In the isolated endothelial cells, using serial confocal cuts through single cells, we regularly noted that FITC-insulin was within the cytosolic compartment and not simply on the cell surface. In tissue sections, we did not find any evidence for FITC-insulin selectively concentrating at punctate sites that might represent intercellular clefts in the wall of vessels. Although we cannot, with these methods, eliminate the possibility that some fraction of insulin movement across the vessel wall occurs via a paracellular route, we found no morphological evidence suggesting such a route. Instead, we provide direct morphological evidence to support the hypothesis that insulin, at physiological concentrations, is taken up by endothelial cells in vivo.

In the present study, we also observed that, both in vivo and in vitro, insulin colocalizes with IR in endothelial cells, suggesting that the insulin binding to its receptor may play a role in insulin's movement into or across the endothelium. This would certainly be consistent with the early observations by King and Johnson (12) that insulin transport displayed saturable kinetics and was inhibited by anti-IR antibodies in cultured endothelial cells. Likewise, in the more physiological setting of the perfused rat heart, when insulin was added to the perfusate at a range of insulin concentrations from $<10^{-10}$ to $\sim10^{-5}$ M, the higher concentration of insulin diminished the amount of ^{125}I-insulin detected in autoradiographs over endothelial cells and muscle interstitium, suggesting saturation kinetics of insulin transport (1). In addition to IR, endothelial cells possess abundant IGF-IR that bind insulin at concentrations in the nanomolar range (5, 13). We (13) and others (5) have recently noted that the endothelial cell, like muscle and adipose, contains "hybrid" receptors composed of one insulin and one IGF-IR αβ-chain in the heterotetramer that would presumably be detected as IR in our micrographs. Both the IGF-I and insulin/IGF-I hybrid receptors could also potentially participate in transendothelial insulin movement. Our observation that both IGF-I and anti-IGF-IR blocking antibody diminish the transport of insulin across endothelial monolayers is consistent with such a role, particularly at high physiological and pharmacological insulin concentrations. IGF-IR are reported to be present at a 10-fold excess relative to IR in endothelial cells (5). Participation by IGF-IR in facilitating insulin transport from the vasculature may explain in part the lack of saturability of insulin transport observed in some in vivo studies (8, 25).

The partial overlap noted in isolated bAECs immunostaining for insulin, IR, and caveolin-1 raises the intriguing question of whether the passage of insulin across the endothelial cell involves vesicular trafficking by caveolae. Schnitzer et al. (20) previously demonstrated that filipin significantly inhibits ^{125}I-insulin transport across monolayers of cultured bAECs. We have confirmed that observation. In addition, we observed that caveolin-1 coprecipitates with the IR (as judged by Western blotting and liquid chromatography-mass spectrometry) and that this occurs in the reciprocal fashion when caveolin-1 is the target of the immunoprecipitation further supports their association in intact endothelial cells. A physical association between IR and caveolin-1 has been reported in adipocytes (7), although not previously in endothelial cells. Indeed, a specific scaffolding domain of caveolin-1 has been suggested to mediate the binding of IR with caveolin-1, and IR are reported to directly tyrosine phosphorylate caveolin-1 and thereby modulate its biological function in adipocytes (11). In adipocytes, colocalization of IR and caveolin-1 has been observed morphologically as well. However, some laboratories question the relationship between caveolae and IR in the adipocyte (6). Our findings are certainly consistent with an interaction between IR and caveolin-1 but do not definitively address whether insulin transits the endothelial cell via a vesicular pathway involving caveolae. Interestingly, IGF-I has also been reported to tyrosine phosphorylate caveolin-1 (15).

In the present study, the FITC-insulin infused in vivo was strikingly concentrated in the vascular endothelial layer of the skeletal muscle within 10 min of beginning the infusion. As noted previously, in perfused heart the endothelium is strongly stained by ^{125}I-insulin within 2 min. It is of interest to consider this rapid uptake by the endothelium in light of a number of reports (16, 17) suggesting that transcapillary insulin transport from the plasma to the interstitial fluid compartment of skeletal muscle may be a rate-limiting step in insulin's peripheral action, as well as reports (16, 17, 32) demonstrating the presence of a gradient between the plasma and muscle interstitium for insulin, suggesting again that transit across the vascular endothelium may be a limiting step for insulin delivery. In the aggregate, our findings are consistent with the endothelial cell being the vascular site of insulin transit across endothelium and with the insulin and/or IGF-IR participating in transendothelial insulin transfer. However, our findings suggest that the uptake of insulin can be very rapid, and it may be insulin transit across the endothelial cell or release at the ablumenal side that normally limits the rate of insulin transfer. Inasmuch as it has been reported (23) that transendothelial transport of insulin is delayed in insulin-resistant obese humans, suggesting that this process might, at least in part, contribute to peripheral insulin resistance, a more detailed kinetic study of these processes appears warranted. However, it also remains possible that, in the insulin-resistant state, the

uptake of insulin by the endothelium might also be slowed, as has been demonstrated for insulin uptake by isolated endothelial cells following an oxidative stress delivered in vitro (3).

GRANTS

This work was supported by National Institute of Diabetes and Digestive and Kidney Diseases Grants DK-38578 and DK-57878 (E. J. Barrett), a research grant from the American Diabetes Association (Z. Liu), and P30-DK-063609 to the University of Virginia Diabetes Endocrinology Research Center. H. Wang was supported by Grant T32-DK-007320-26.

REFERENCES

1. **Bar RS, Boes M, and Sandra A.** Vascular transport of insulin to rat cardiac muscle. Central role of the capillary endothelium. *J Clin Invest* 81: 1225–1233, 1988.
2. **Bendayan M and Rasio EA.** Transport of insulin and albumin by the microvascular endothelium of the rete mirabile. *J Cell Sci* 109: 1857–1864, 1996.
3. **Bertelsen M, Anggard EE, and Carrier MJ.** Oxidative stress impairs insulin internalization in endothelial cells in vitro. *Diabetologia* 44: 605–613, 2001.
4. **Castillo C, Bogardus C, Bergman R, Thuillez P, and Lillioja S.** Interstitial insulin concentrations determine glucose uptake rates but not insulin resistance in lean and obese men. *J Clin Invest* 93: 10–16, 1994.
5. **Chisalita SI and Arnqvist HJ.** Insulin-like growth factor I receptors are more abundant than insulin receptors in human micro- and macrovascular endothelial cells. *Am J Physiol Endocrinol Metab* 286: E896–E901, 2004.
6. **Cohen AW, Combs TP, Scherer PE, and Lisanti MP.** Role of caveolin and caveolae in insulin signaling and diabetes. *Am J Physiol Endocrinol Metab* 285: E1151–E1160, 2003.
7. **Gustavsson J, Parpal S, Karlsson M, Ramsing C, Thorn H, Borg M, Lindroth M, Peterson KH, Magnusson KE, and Stralfors P.** Localization of the insulin receptor in caveolae of adipocyte plasma membrane. *FASEB J* 13: 1961–1971, 1999.
8. **Hamilton-Wessler M, Ader M, Dea MK, Moore D, Loftager M, Markussen J, and Bergman RN.** Mode of transcapillary transport of insulin and insulin analog NN304 in dog hindlimb: evidence for passive diffusion. *Diabetes* 51: 574–582, 2002.
9. **Holmang A, Mimura K, Bjorntorp P, and Lonnroth P.** Interstitial muscle insulin and glucose levels in normal and insulin-resistant Zucker rats. *Diabetes* 46: 1799–1804, 1997.
10. **Jansson PA, Fowelin JP, von Schenck HP, Smith UP, and Lonnroth PN.** Measurement by microdialysis of the insulin concentration in subcutaneous interstitial fluid. Importance of the endothelial barrier for insulin. *Diabetes* 42: 1469–1473, 1993.
11. **Kimura A, Mora S, Shigematsu S, Pessin JE, and Saltiel AR.** The insulin receptor catalyzes the tyrosine phosphorylation of caveolin-1. *J Biol Chem* 277: 30153–30158, 2002.
12. **King GL and Johnson SM.** Receptor-mediated transport of insulin across endothelial cells. *Science* 227: 1583–1586, 1985.
13. **Li G, Barrett EJ, Wang H, Chai W, and Liu Z.** Insulin at physiological concentrations selectively activates insulin but not insulin-like growth factor I (IGF-I) or insulin/IGF-I hybrid receptors in endothelial cells. *Endocrinology* 146: 4690–4696, 2005.
14. **Long W, Barrett EJ, Wei L, and Liu Z.** Adrenalectomy enhances the insulin sensitivity of muscle protein synthesis. *Am J Physiol Endocrinol Metab* 284: E102–E109, 2003.
15. **Maggi D, Biedi C, Segat D, Barbero D, Panetta D, and Cordera R.** IGF-I induces caveolin 1 tyrosine phosphorylation and translocation in the lipid rafts. *Biochem Biophys Res Commun* 295: 1085–1089, 2002.
16. **Miles PD, Levisetti M, Reichart D, Khoursheed M, Moossa AR, and Olefsky JM.** Kinetics of insulin action in vivo. Identification of rate-limiting steps. *Diabetes* 44: 947–953, 1995.
17. **Miles PD, Li S, Hart M, Romeo O, Cheng J, Cohen A, Raafat K, Moossa AR, and Olefsky JM.** Mechanisms of insulin resistance in experimental hyperinsulinemic dogs. *J Clin Invest* 101: 202–211, 1998.
18. **Noguchi M, Furuya S, Takeuchi T, and Hirohashi S.** Modified formalin and methanol fixation methods for molecular biological and morphological analyses. *Pathol Int* 47: 685–691, 1997.
19. **Rattigan S, Clark MG, and Barrett EJ.** Hemodynamic actions of insulin in rat skeletal muscle: Evidence for capillary recruitment. *Diabetes* 46: 1381–1388, 1997.
20. **Schnitzer JE, Oh P, Pinney E, and Allard J.** Filipin-sensitive caveolae-mediated transport in endothelium: reduced transcytosis, scavenger endocytosis, and capillary permeability of select macromolecules. *J Cell Biol* 127: 1217–1232, 1994.
21. **Segal SS, Brett SE, and Sessa WC.** Codistribution of NOS and caveolin throughout peripheral vasculature and skeletal muscle of hamsters. *Am J Physiol Heart Circ Physiol* 277: H1167–H1177, 1999.
22. **Simionescu M, Gafencu A, and Antohe F.** Transcytosis of plasma macromolecules in endothelial cells: a cell biological survey. *Microsc Res Tech* 57: 269–288, 2002.
23. **Sjostrand M, Gudbjornsdottir S, Holmang A, Lonn L, Strindberg L, and Lonnroth P.** Delayed transcapillary transport of insulin to muscle interstitial fluid in obese subjects. *Diabetes* 51: 2742–2748, 2002.
24. **Sjöstrand M, Holmäng A, and Lönnroth P.** Measurement of interstitial insulin in human muscle. *Am J Physiol Endocrinol Metab* 276: E151–E154, 1999.
25. **Steil GM, Ader M, Moore DM, Rebrin K, and Bergman RN.** Transendothelial insulin transport is not saturable in vivo. No evidence for a receptor-mediated process. *J Clin Invest* 97: 1497–1503, 1996.
26. **Vincent MA, Clerk LH, Lindner JR, Klibanov AL, Clark MG, Rattigan S, and Barrett EJ.** Microvascular recruitment is an early insulin effect that regulates skeletal muscle glucose uptake in vivo. *Diabetes* 53: 1418–1423, 2004.
27. **Vincent MA, Clerk LH, Rattigan S, Clark MG, and Barrett EJ.** Active role for the vasculature in the delivery of insulin to skeletal muscle. *Clin Exp Pharmacol Physiol* 32: 302–307, 2005.
28. **Wallis MG, Wheatley CM, Rattigan S, Barrett EJ, Clark AD, and Clark MG.** Insulin-mediated hemodynamic changes are impaired in muscle of Zucker obese rats. *Diabetes* 51: 3492–3498, 2002.
29. **Wang H, Germanson TP, and Guyenet PG.** Depressor and tachypneic responses to chemical stimulation of the ventral respiratory group are reduced by ablation of neurokinin-1 receptor-expressing neurons. *J Neurosci* 22: 3755–3764, 2002.
30. **Wang H, Stornetta RL, Rosin DL, and Guyenet PG.** Neurokinin-1 receptor-immunoreactive neurons of the ventral respiratory group in the rat. *J Comp Neurol* 434: 128–146, 2001.
31. **Yang YJ, Hope I, Ader M, Poulin RA, and Bergman RN.** Dose-response relationship between lymph insulin and glucose uptake reveals enhanced insulin sensitivity of peripheral tissues. *Diabetes* 41: 241–253, 1992.
32. **Yang YJ, Hope ID, Ader M, and Bergman RN.** Insulin transport across capillaries is rate limiting for insulin action in dogs. *J Clin Invest* 84: 1620–1628, 1989.
33. **Zhang L, Vincent MA, Richards SM, Clerk LH, Rattigan S, Clark MG, and Barrett EJ.** Insulin sensitivity of muscle capillary recruitment in vivo. *Diabetes* 53: 447–453, 2004.